Cone-Beam Computed Tomography and Deformable Registration-Based "Dose of the Day" Calculations for Adaptive Proton Therapy

Catarina Veiga, MSc[1]; Jailan Alshaikhi, MSc[1,2]; Richard Amos, MSc[2]; Ana Mónica Lourenço, MSc[1,3]; Marc Modat, PhD[4]; Sebastien Ourselin, PhD[4]; Gary Royle, PhD[1]; Jamie R. McClelland, PhD[4]

[1]Radiation Physics Group, Department of Medical Physics and Biomedical Engineering, University College London, London WC1E 6BT, UK
[2]Department of Radiotherapy Physics, University College London Hospital, London NW1 2PG, UK
[3]Ionizing Radiation Team, National Physical Laboratory, Teddington TW11 0LW, UK
[4]Centre for Medical Image Computing, Department of Medical Physics and Biomedical Engineering, University College London, London WC1E 6BT, UK

Abstract

Purpose: The aim of this work was to evaluate the feasibility of cone-beam computed tomography (CBCT) and deformable image registration (DIR)–based "dose of the day" calculations for adaptive proton therapy.

Methods: Intensity-modulated radiation therapy (IMRT) and proton therapy plans were designed for 3 head and neck patients that required replanning, and hence had a replan computed tomography (CT). Proton plans were generated for different beam arrangements and optimizations: intensity modulated proton therapy and single-field uniform dose. We used an in-house DIR software implemented at our institution to generate a deformed CT, by warping the planning CT onto the daily CBCT. This CBCT had a similar patient geometry to the replanned CT. Dose distributions on the replanned CT were considered the gold standard for "dose of the day" calculations, and were compared with doses on deformed CT (our method) and directly on the calibrated CBCT and rigidly aligned planning CT (alternative methods) in terms of dose difference (DD), by calculating the percentage of voxels whose DD was smaller than 2% of the prescribed dose ($DD_{2\%\text{-}pp}$) and the root mean square of the DD distribution (DD_{RMS}).

Results: Using a deformed CT, the $DD_{2\%\text{-}pp}$ within the CBCT imaging volume was 93.2% ± 0.7% for IMRT, and 87% ± 3% for proton plans. In a region of higher dose gradient, we found that although $DD_{2\%\text{-}pp}$ was 94.3% ± 0.2% for IMRT, in proton plans, it dropped to 74% ± 4%. A larger number of treatment beams and single-field uniform dose optimization appear to make the proton plans less sensitive to DIR errors. For example, within the treated volume, the DD_{RMS} was reduced from 2.6% ± 0.6% of the prescribed dose to 1.0% ± 1.3% of the prescribed dose when using single-field uniform dose optimization.

Conclusions: Promising results were found for DIR- and CBCT-based proton dose calculations. Proton dose calculations were, however, more sensitive to registration errors than IMRT doses were, particularly in high dose gradient regions.

Keywords: adaptive radiation therapy; cone-beam computed tomography; deformable image registration; head and neck cancer

Submitted 03 Nov 2014
Accepted 28 May 2015
Published 16 Oct 2015

Corresponding author:
Catarina Veiga, MSc
Department of Medical Physics and Biomedical Engineering
Malet Place Engineering Building
Gower Street,
London WC1E 6BT, UK
Phone: +44 20 7679 0200
catarina.veiga.11@ucl.ac.uk

Original Article

DOI
10.14338/IJPT-14-00024.1

http://theijpt.org

Introduction

Volumetric imaging has proven to be extremely valuable for patient positioning and daily monitoring of anatomic changes during photon treatments, particularly for patients with head and neck malignancies. The anatomy is known to change during the course of the treatment [1], and it can compromise the dosimetric objectives of the original photon plan [2]. Adaptive radiation therapy approaches that use in-room imaging techniques, such as computed tomography (CT) on-rails and cone-beam CT (CBCT), are becoming increasingly popular in state-of-art photon therapy care [3]. Moreover, CBCT has some advantages over in-room CT scanners: the patient does not need to be moved between scanning and treatment, the extra imaging dose burden is smaller, and CBCT scanners are a more cost-efficient equipment for image guidance. However, CBCT image quality is not reliable for direct-dose calculations [4].

Interest has recently increased in translating existing 3-dimensional photon imaging technology, particularly CBCT, into the proton clinic. The development of CBCT in proton therapy systems requires solving engineering problems related with the geometry of a proton gantry. Seabra et al [5] describe the major challenges for CBCT integration in a proton gantry compared with a linear accelerator. Such challenges include higher thermal capacity x-ray tubes being necessary because of the larger source to isocenter distance of a proton gantry. Several groups are currently commissioning CBCT systems for clinical use in proton therapy [5–7] in collaboration with manufacturers that already advertise such products with their proton-therapy solutions. The only reliable alternative for 3-dimensional imaging before treatment is in-room CT, which is not widely available [8].

Numerous published reports have documented the theoretic [9–12] advantages of, and clinical evidence [13–17] for, the benefits of proton therapy over photon therapy for head and neck malignancies. It is possible with proton therapy to achieve decreased dose to the optic nerves, the parotid glands, and the oral cavity, leading to fewer feeding tubes being used. This reduction is accomplished without compromising the conformity index, dose homogeneity, and coverage of the target volume [18]. Although theoretically protons have dosimetric advantages versus photons, to fully take advantage of the potential of proton therapy and achieve clinical benefit, the variations in anatomy (such as weight loss and tumor shrinkage) have to be monitored and accounted for, similar to that in photon therapy [19].

Work conducted previously by our group demonstrated the feasibility of using deformable image registration (DIR) to map the Hounsfield units (HUs) from the CT to the geometry of the daily CBCT. This method provided a good estimation of the "dose of the day" for intensity modulated radiation therapy (IMRT) treatments [20], which can be used to feed an adaptive radiation therapy workflow. However, the challenges found in conventional photon therapy are even more concerning for proton therapy, and this approximation may no longer be valid for proton therapy mainly for 2 reasons. First, because the dose gradient in proton dose distributions is steeper, accurate positioning is even more crucial to minimize the risk of overdosing organs at risk (OARs) and/or underdosing target volumes. Additionally, fraction to fraction changes in size and position of tissue heterogeneities will adversely affect the dose distribution properties of protons to a greater extent than with photons because proton dose-depth curves are more dependent on the physical properties of the tissue than photons are. In the head and neck region, the changes can be complex because protons travel through a complex anatomy composed of air, bone, and soft tissues [11]. Proton dose calculations are, therefore, expected to be more sensitive to registration errors than analogous IMRT cases. The aim of this work was to evaluate the feasibility of a CBCT- and DIR-based "dose of the day" calculation for adaptive proton therapy, which was previously evaluated for IMRT treatments. A more sophisticated and improved registration algorithm was used in this study.

Methods

Patient Data and Imaging

Data from 3 patients with head and neck cancer treated at our institution were used retrospectively for this study. All patients underwent CT for treatment planning (GE Widebore 16 slice system, GE Healthcare, Little Chalfont, UK) and weekly CBCT for verification (On-Board Imaging v1.4, Varian Medical Systems, Palo Alto, California). The CBCTs were acquired in half-fan mode, full rotation, 110 kVp, 20 mA, 20 ms, with a maximum field-of-view (FoV) of 45 cm in diameter, and 16 cm in length (4-6 mSv per scan). The patients included in this study also had a replan CT (rCT) because large anatomic changes were observed during treatment that compromised the treatment objectives; therefore, a replan was necessary. Thus, the patients selected benefit from adaptive radiation therapy approaches and were challenging cases for DIR. Imaging resolution was $0.977 \times 0.977 \times 2.5$ mm for the CTs, whereas the CBCT corresponded to $0.879 \times 0.879 \times 2$ mm with a maximum of 16 cm in

length. A customized thermoplastic mask and headrest were used for immobilization. The rCT was acquired with a new mask that attempted to reproduce the previous immobilization as closely as possible.

For the rCT and CBCT to contain the same information, they should ideally be acquired at the same time and positioning. In practice, such a data set is not easily available because not only there is no clinical benefit in acquiring both scans on the same day but also there would still exist residual differences from moving the patient between imaging systems. The first CBCT we had available clinically with the patient in the same treatment position was acquired 5–7 days after the rCT. To deal with the nonnegligible geometric differences between the rCT and the CBCT, we generated a simulated CBCT by deforming the real CBCT to match the rCT. This step was carefully evaluated patient by patient to maximize the similarity between rCT and CBCT and thus to minimize the errors in dose estimation because of such discrepancies. The simulated CBCT was used both for DIR and direct-dose calculations.

Treatment Planning

The choice of beams was to optimize target coverage while minimizing dose to the brainstem, spinal canal, oral cavity, salivary glands, and larynx. The same prescribed doses and volumes were used in all treatment approaches: 65 Gy (relative biological effectiveness [RBE]) to the primary disease and 54 Gy (RBE) to the secondary disease were planned for delivery in 30 fractions. The planning target volumes (PTVs) were defined as a 3 mm expansion of the clinical target volumes. The primary objective of the plans was to achieve 95% of the prescribed dose to the PTV while maximizing conformity. The plans were then optimized to minimize the dose to the OARs without compromising target coverage. Tolerance doses followed the University College London Hospital guidelines for IMRT treatments: maximum doses of 46 Gy (RBE) and 55 Gy (RBE) to the spinal canal and brainstem, and mean unilateral dose of 20 Gy (RBE) and bilateral dose of 25 Gy (RBE) to the parotid glands.

Treatment planning was performed on the planning CT (pCT) scan using the Eclipse External Beam planning system (version 10.8, Varian Medical Systems, Palo Alto, California). For IMRT cases, the patients were planned as part of our clinical workflow using a 7-field protocol, and they were treated with the plans used in this study. Proton treatment planning was done retrospectively, with the plans generated per patient consisting of 2 types of optimization: intensity-modulated proton therapy (IMPT) and single-field uniform dose (SFUD), and 2 different beam arrangements: 3 beams with gantry rotations of 60°, 180°, and 300° and 5 beams with gantry rotations of 45°, 135°, 180°, 225°, and 315°. A total of 3 plans were generated, IMPT with 3 and 5 beams ($IMPT_{3B}$ and $IMPT_{5B}$) and SFUD with 3 beams ($SFUD_{3B}$). The $IMPT_{3B}$ represents a standard curative approach, which maximizes the potential benefits of proton therapy (ie, reduced integral dose, minimized dose to OARs, and greater homogeneity inside the PTV) [12, 17]. However, such plans can be sensitive to positioning errors and anatomic changes. In contrast, $IMPT_{5B}$ and $SFUD_{3B}$ are more robust planning strategies at the cost of smaller dosimetric benefits. Particularly, $SFUD_{3B}$ reduced the ability to minimize the maximum dose to the canal because all the fields have similar weight, whereas $IMPT_{5B}$ increased the integral dose. **Table 1** presents the dose statistics and properties of the plans, such as mean and maximum doses to OARs, conformity index [21], homogeneity index [22], and nontarget integral dose [23]. The focus of this article is not treatment planning; therefore, the proton plans were designed to be clinically acceptable and to demonstrate the benefits of proton therapy, and not necessarily to be optimal (**Figure 1**).

Image Registration

We registered the pCT to the simulated CBCT using the open-source registration package implemented at our institution, NiftyReg (http://cmic.cs.ucl.ac.uk/home/software/). NiftyReg includes several B-spline free-form deformation-based algorithms [24], and we opted to use the implementation based on the stationary velocity-field transformation model [25]. This is a symmetric and inverse-consistent algorithm, which provides both the forward and inverse transformations. The localized normalized cross-correlation was used as a similarity measure because it is well suited to account for the differences in image intensities between CT and CBCT. Because the localized normalized cross-correlation calculates the similarity over local windows, rather than the whole volume, it can better account for the spatially varying intensity values in CBCT imaging than global similarity measures, such as the normalized cross-correlation or the sum of squared differences. Bending energy was used as a regularization term [24]. More details on the registration's optimization and validation can be found elsewhere [20, 26].

The reduced length in the superior-inferior direction of the CBCT scans often makes the images unusable for dose calculations. In our previous work [20], we proposed a method to handle this limitation that estimates the deformation, and hence the volume, outside the CBCT FoV as a smooth transition between the initial rigid alignment and the deformation optimized during the DIR inside the imaging volume. We found this approximation reliable for IMRT treatments, but mostly in

Table 1. Mean ± SD of the dose statistics and properties of the plans used in this study.

	IMRT	$IMPT_{3B}$	$SFUD_{3B}$	$IMPT_{5B}$
Spinal canal				
D_{mean} [Gy (RBE)]	28 ± 4	13 ± 2	20.5 ± 1.4	11 ± 3
D_{max} [Gy (RBE)]	41 ± 2	33 ± 4	42 ± 2	28 ± 3
Brainstem				
D_{mean} [Gy (RBE)]	14 ± 6	7 ± 4	7 ± 4	5.6 ± 1.0
D_{max} [Gy (RBE)]	38 ± 9	29 ± 9	24 ± 11	25 ± 4
Left parotid				
D_{mean} [Gy (RBE)]	40 ± 7	29 ± 5	34 ± 5	29 ± 4
D_{max} [Gy (RBE)]	63 ± 5	63 ± 4	64 ± 4	64 ± 5
Right parotid				
D_{mean} [Gy (RBE)]	43 ± 6	33 ± 2	37.8 ± 0.7	33.3 ± 1.6
D_{max} [Gy (RBE)]	67.1 ± 1.6	66.8 ± 0.4	67.1 ± 0.1	66.9 ± 0.4
Conformity index[a]	0.87 ± 0.02	0.81 ± 0.06	0.88 ± 0.03	0.80 ± 0.05
Homogeneity index[b]	1.08 ± 0.02	1.08 ± 0.03	1.10 ± 0.02	1.10 ± 0.07
Integral dose[c] (Gy × *L*)	160 ± 40	120 ± 20	120 ± 20	130 ± 20

Abbreviations: 3B, 3-beam; 5B, 5-beam; D_{max}, maximum dose; D_{mean}, mean dose; IMPT, intensity-modulated proton therapy; IMRT, intensity-modulated radiation therapy; RBE, relative biological effectiveness; SFUD, single-field uniform dose.

[a]Confidence interval = $V_{PTV} \cap V_{95\%}/V_{95\%}$, where V_{PTV} is the volume of the planning target volume, and $V_{95\%}$ is the volume of the 95% isodose level.

[b]Hetogeneity index = $D_{5\%}/D_{95\%}$, where $D_{5\%}$ and $D_{95\%}$ are the doses received by 5% and 95% of the planning target volume.

[c]Integral dose = $V_{NTV} \times D_{mean}$, where V_{NTV} is the nontarget volume, and D_{mean} is mean dose.

the superior direction, where the anatomy moves rigidly. However, the limited FoV is expected to be more problematic in proton therapy, so the suitability of this approximation was also evaluated in this work.

Dose Comparison

We used the DIR to map the HU from the pCT to a CBCT that closely resembled the rCT (the simulated CBCT described in the Patient Data and Imaging section). This process results in a deformed CT (dCT) that has the geometric information of the CBCT but the HU values from the pCT and can, therefore, be used for accurate dose calculations.

A dosimetric evaluation was performed to evaluate the effect of the registration errors in calculating the "dose of the day." **Figure 2** shows a diagram of the images used in this study and the corresponding dose calculations performed. Dose distributions calculated on rCT were considered the gold standard and were compared with doses on dCT (our method) and directly with the calibrated CBCT and rigidly aligned pCT (alternative methods). The calibrated CBCT refers to the simulated

Figure 1. Dose-volume histogram comparing intensity-modulated radiation therapy and proton plans for one of the patients included in this study. Right parotid omitted for figure clarity.

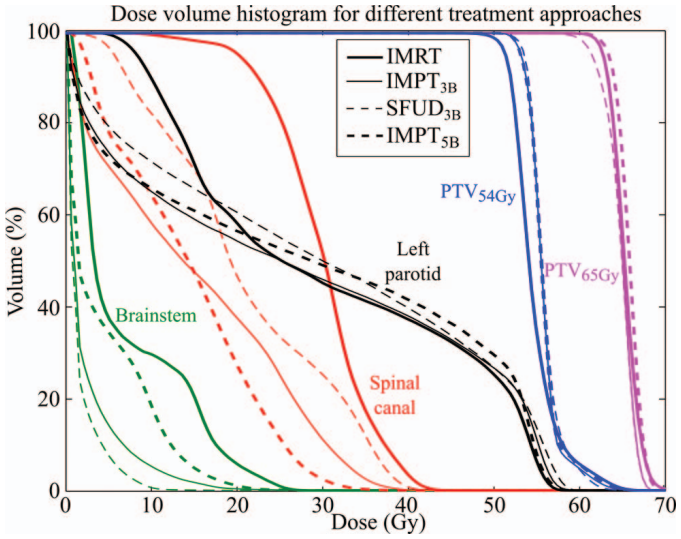

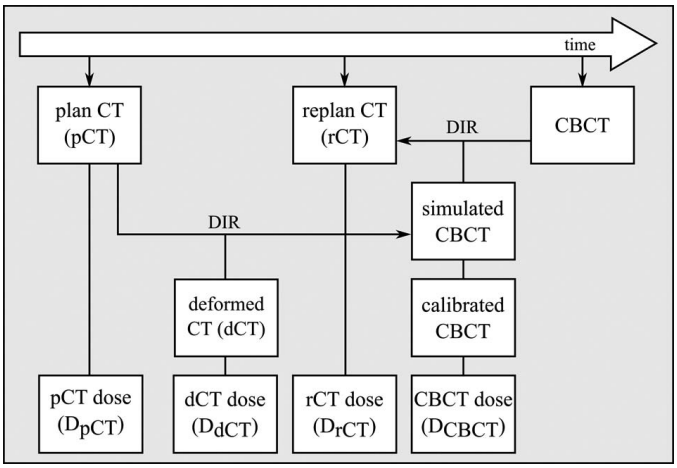

Figure 2. Diagram of the imaging data used and respective dose calculations. The pCT was deformed onto a CBCT that closely resembled the rCT. This was a simulated CBCT that resulted from deforming the real CBCT to match the rCT. Dose distributions for the same photon and proton plans were calculated on the rigidly aligned pCT, rCT, dCT, and calibrated CBCT (D_{pCT}, D_{rCT}, D_{dCT}, and D_{CBCT}, respectively). Abbreviations: CBCT, cone-beam computed tomography; CT, computed tomography; dCT, deformed computed tomography; pCT, planning computed tomography; rCT, replan computed tomography.

CBCT after its HU values were corrected using a quadratic relationship between CT and CBCT measured with the Catphan-504 (Phantom Laboratory, Greenwich, New York). Finally, the calibrated CBCT was also extended in the superior-inferior direction using the corresponding rigidly aligned pCT slices [20]. Therefore, dose distributions for the same IMRT and proton plans were calculated on the pCT, rCT, dCT, and the calibrated CBCT (D_{pCT}, D_{rCT}, D_{dCT}, and D_{CBCT}, respectively). The isocenter was placed in the same point in both cases based on rigid alignment of the vertebrae. All doses were calculated with a resolution of 2 mm.

The uncertainty of the dose calculations was evaluated by computing the voxelwise difference between dose distributions, known as the dose difference (DD) test. The DD results were assessed calculating the DD-test pass percentage using a tolerance of 2% of the prescribed dose (pD) (ie, the percentage of pixels whose DD was within tolerance [$DD_{2\%\text{-}pp}$]) and the root mean square of the DD distribution (DD_{RMS}). Additionally, we computed the dose-volume histograms and the differences in calculating the mean and maximum doses (ΔD_{mean} and ΔD_{max}) to OARs.

Results

Table 2 provides the results obtained for $DD_{2\%\text{-}pp}$ and DD_{RMS} between the different methods and the rCT within different regions of interest. Because of the anatomic changes, the pCT does not give a good estimate of the dose of the day, particularly for proton plans. Dose calculations on the calibrated CBCT also result in a poor estimation of the "dose of the day" in spite of the images closely representing the anatomy of the day. Visual inspection of the DD maps revealed that the major source of dose mismatch was within regions in which the CBCT imaging quality was degraded (such as near the shoulders where the imaging volume is larger [27]). In such larger volumes, a single calibration curve failed to recover the correct HU, resulting in inaccurate dose calculations. Proton plans were, therefore, more sensitive both to anatomic changes and to the inconsistency in the HU characteristic of the CBCT imaging than were the photon plans. The errors in the "dose of the day" calculations on the dCT were also larger for the proton plans than they were for the IMRT plans but, in all cases, were considerably lower than for the calibrated CBCT and rigidly aligned pCT.

Different regions of the dose map were more sensitive to registration errors. The $DD_{2\%\text{-}pp}$ differences between the volume encompassed by the planning 95% isodose surface (the treated volume [TV]) and the volume receiving 50% to 95% of the prescribed dose (the irradiated volume [IV] minus the TV [IV − TV]), where higher gradients are more likely to occur, indicate that the local properties of the dose map affect the accuracy of the "dose of the day" calculations. Proton plans were also more sensitive than photon plans were to higher dose gradients. For example, for $IMPT_{3B}$, the DD_{RMS} was 2.6% ± 0.6% of the pD within the TV, and that value increased to 8.2% ± 0.4% of the pD within the IV − TV. Similar behavior was found for all the plans, but in the IMRT, the DD_{RMS} was considerably lower (0.57% ± 0.09% of the pD and 3.1% ± 0.3% of the pD for TV and IV − TV, respectively). **Figure 3** provides a qualitative view of this effect. Although, in IMRT, most errors occurred near the skin and airways, in proton plans, the differences were larger within the high dose and dose-gradient regions. Additionally, in the proton plans, the $DD_{2\%\text{-}pp}$ outside the imaging FoV was consistently smaller than within the CBCT FoV, unlike the IMRT case. This is indicative that whereas using the pCT outside the imaging FoV was a valid approximation for proton treatments (particularly in the superior direction), special care is needed if high-dose gradients occur outside the imaging FoV.

Table 2. Mean ± SD of the $DD_{2\%\text{-pp}}$ and DD_{RMS} between doses calculated using a rigidly aligned planning CT, calibrated CBCT and deformed CT in comparison with a replan CT within different regions of interest. The CBCT and nonimaged FoV stand for the regions where more than 10% of the prescribed dose was deposited that were imaged or not, respectively. The TV corresponds to the volume encompassed by the planning 95% isodose surface, while the IV corresponds to the volume encompassed by the planning 50% isodose surface. Therefore IV-TV is the volume where 50 to 95% of the dose was planned to be delivered.

	Nonimaged FoV		CBCT FoV		TV		IV-TV	
	$DD_{2\%\text{-pp}}$ (%)	DD_{RMS} (%pD)	$DD_{2\%\text{-pp}}$ (%)	DD_{RMS} (%pD)	$DD_{2\%\text{-pp}}$ (%)	DD_{RMS} (%pD)	$DD_{2\%\text{-pp}}$ (%)	DD_{RMS} (%pD)
IMRT								
D_{pCT}	92.3 ± 1.2	2.5 ± 0.2	72 ± 6	8.6 ± 1.1	64 ± 16	4.6 ± 1.6	73 ± 5	8 ± 3
D_{CBCT}	89 ± 4	2.1 ± 0.2	74 ± 3	3.5 ± 0.3	84 ± 9	1.8 ± 1.6	62 ± 5	4.0 ± 0.7
D_{dCT}	96.0 ± 0.6	1.5 ± 0.4	93.2 ± 0.7	2.5 ± 0.2	99.1 ± 0.4	0.57 ± 0.09	94.3 ± 0.2	3.1 ± 0.3
$IMPT_{3B}$								
D_{pCT}	59 ± 12	5.9 ± 1.1	51 ± 4	10 ± 3	49 ± 9	6.0 ± 1.7	32 ± 8	14 ± 4
D_{CBCT}	65 ± 7	5.2 ± 1.5	62 ± 3	6.7 ± 0.9	72 ± 5	3.3 ± 0.5	44 ± 2	9.9 ± 1.5
D_{dCT}	76 ± 6	3.3 ± 0.8	85 ± 2	4.0 ± 0.1	88.8 ± 0.3	2.6 ± 0.6	71.1 ± 1.1	8.2 ± 0.4
$SFUD_{3B}$								
D_{pCT}	67 ± 8	4.9 ± 1.1	62 ± 2	9 ± 2	81 ± 8	2.7 ± 0.8	43 ± 11	12 ± 3
D_{CBCT}	69 ± 7	4.3 ± 1.1	69.7 ± 0.8	6.1 ± 0.5	91 ± 4	1.4 ± 0.5	54 ± 5	8.3 ± 0.9
D_{dCT}	80 ± 3	2.8 ± 0.6	87 ± 2	3.4 ± 0.2	97.7 ± 0.8	1.0 ± 0.3	76 ± 5	7.1 ± 0.5
$IMPT_{5B}$								
D_{pCT}	65 ± 9	5.0 ± 1.2	57 ± 8	9 ± 3	52 ± 11	7 ± 3	36 ± 7	11 ± 4
D_{CBCT}	68 ± 4	4.4 ± 0.5	66 ± 3	5.8 ± 0.8	76 ± 8	3.2 ± 1.1	44.7 ± 0.8	8.6 ± 1.0
D_{dCT}	79.3 ± 0.4	2.9 ± 0.3	88 ± 3	3.5 ± 0.2	91 ± 4	2.5 ± 0.5	75 ± 3	7.0 ± 0.7

Abbreviations: 3B, 3-beam; 5B, 5-beam; %pD, percentage of the prescribed dose; CBCT, cone-beam computed tomography; CT, computed tomography; $DD_{2\%\text{-pp}}$, dose difference test pass-percentage (pass criteria of 2% of the prescribed dose); D_{CBCT}, dose distribution of the calibrated cone-beam computed tomography; D_{dCT}, dose distribution of the deformed computed tomography; D_{pCT}, dose distribution in the planning computed tomography; DD_{RMS}, root mean square of the dose difference distribution; FoV, field-of-view; IMPT, intensity-modulated proton therapy; IMRT, intensity-modulated radiation therapy; IV, irradiated volume; SFUD, single-field uniform dose; TV, treated volume.

Different optimization and delivery techniques for the proton plans resulted in different $DD_{2\%\text{-pp}}$ and DD_{RMS}. The $IMPT_{3B}$ was more sensitive to DIR errors, particularly within IV − TV. The $SFUD_{3B}$ performed particularly well within the TV because all fields delivered a uniform dose to the high-dose region, making it less sensitive to DIR errors. In general, the $IMPT_{5B}$ also performed better than $IMPT_{3B}$ did because less dose was delivered outside the target per beam. The DIR method appears to perform better in photon cases, whereas SFUD optimization and/or additional IMPT beams also lead to better performance.

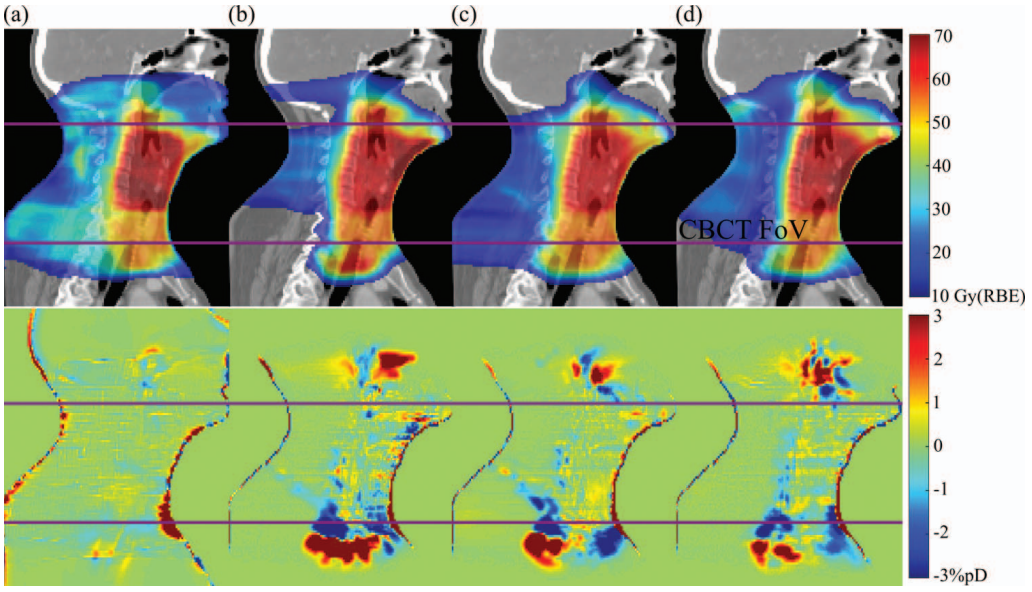

Figure 3. Dose color wash overlayed on the replan CT (top row) and difference in dose between replan CT and deformed CT (bottom row) for (A) the IMRT plan, (B) the $IMPT_{3B}$ plan, (C) the $SFUD_{3B}$ plan, and (D) the $IMPT_{5B}$ plan for one of the patients included in this study. The horizontal purple lines indicate the length of the CBCT FoV. Abbreviations: CBCT, cone-beam computed tomography; CT, computed tomography; FoV, field of view; IMPT, intensity-modulated radiation therapy; IMRT, intensity-modulated radiation therapy; SFUD, single-field uniform dose.

Table 3. Mean ± SD of $DD_{2\%-pp}$, DD_{RMS}, ΔD_{mean}, and ΔD_{max} to OARs (spinal canal, brainstem, and parotids) when using the deformed CT to calculate the "dose of the day" (as a percentage of the pD).

	$DD_{2\%-pp}$ (%)	DD_{RMS} (%pD)	ΔD_{mean} (%pD)	ΔD_{max} (%pD)
IMRT	99.9 ± 0.1	0.3 ± 0.1	0.1 ± 0.1	0.2 ± 0.1
$IMPT_{3B}$	81 ± 17	2.3 ± 1.6	0.8 ± 0.9	1.8 ± 1.7
$SFUD_{3B}$	85 ± 12	1.6 ± 0.8	0.5 ± 0.5	1.3 ± 2.5
$IMPT_{5B}$	80 ± 21	3 ± 3	1.4 ± 2.0	1.8 ± 1.6

Abbreviations: ΔD_{max}, difference in maximum dose; ΔD_{mean}, difference in mean dose; 3B, 3-beam; 5B, 5-beam; %pD, percentage of the prescribed dose; CT, computed tomography; $DD_{2\%-pp}$, dose difference test pass-percentage (pass criteria of 2% of the prescribed dose); DD_{RMS}, root mean square of the dose differences; IMPT, intensity-modulated proton therapy; IMRT, intensity-modulated radiation therapy; OARs, organs at risk; pD, prescribed dose; SFUD, single-field uniform dose.

Table 3 presents the results for D_{dCT} within the OARs. The same trend of better results being obtained for photon plans was observed here. The larger standard deviation found for $DD_{2\%-pp}$ in proton plans is due to the relative positioning of the different OARs in the dose map for each patient. For $IMPT_{3B}$, the $DD_{2\%-pp}$ was 94% ± 6% for the brainstem and spinal canal and 68% ± 14% for the parotids. In general, the parotids have the worst results because of being partially within the TV and, therefore, being more susceptible to high doses and high-dose gradients. One of advantages of using DIR to generate a dCT is to also generate deformed contours automatically, removing the need to delineate all the regions of interest from scratch. The differences when plotting the dose-volume histograms were small when the manual structure set was considered. If the pCT structures were used to generate deformed contours in the dCT, the differences between the curves became more evident (**Figure 4**). The same trend was also found for IMRT plans. The variability in OAR contouring has a significant role when evaluating the need to replan, independent of the treatment modality; therefore, consistent delineations between time points are important for adaptive radiation therapy.

Discussion

Although CBCT imaging is a common imaging modality in photon therapy, it is still in its infancy in proton therapy. With CBCT becoming clinically available, it becomes important to understand how to use it for treatment adaptation and what the inherent uncertainties associated with it are. We evaluated a DIR-based adaptive radiation-therapy workflow that uses doses recalculated in a deformed geometry. Very recent studies by Landry et al [28, 29] also evaluated DIR- and CBCT-based proton-dose calculations on a deformable phantom and patient data, but unlike this work, those studies were less focused on the dosimetric implications and the effect of different treatment strategies. Calculating the "dose of the day" directly on the CBCT was extensively studied for photon therapy [27, 30]. Both approaches can benefit from further refining because of the greater accuracy required for proton-therapy applications. We found that using dCT was more accurate than using a calibrated CBCT approach. Visual inspection of the doses obtained showed that larger imaging volumes have greater noise and less

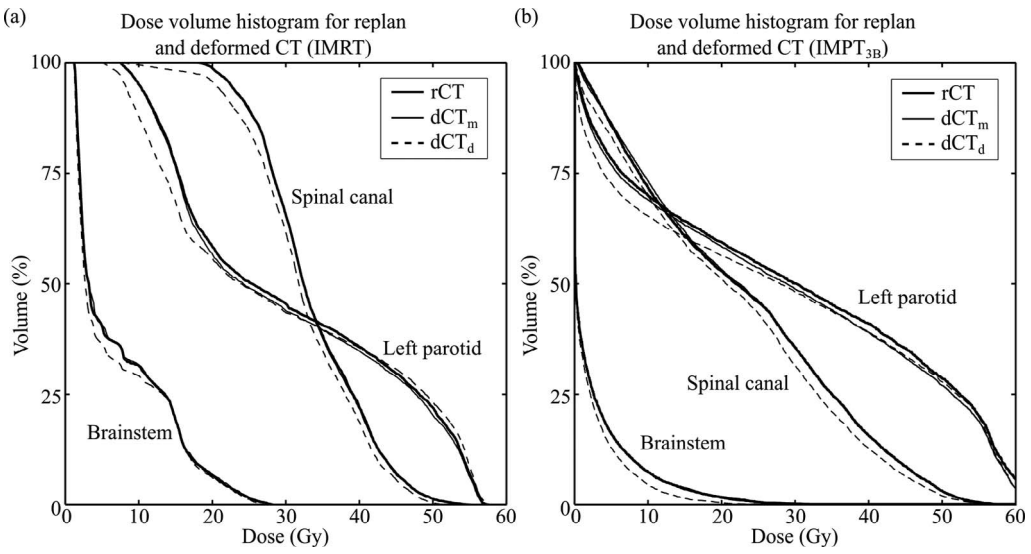

Figure 4. Dose-volume histogram comparing dose in rCT and deformed CT for (A) IMRT and (B) $IMPT_{3B}$ using dCT_m and dCT_d structures, for one of the patients included in this study. Right parotid omitted for figure clarity. Abbreviations: CT, computed tomography; dCT_d, deformed computed tomography (with manually delineated structures); dCT_m, manual deformed computed tomography (with automatically deformed structures); IMPT, intensity-modulated proton therapy; IMRT, intensity-modulated radiation therapy; rCT, replan computed tomography.

contrast and are the main source of errors in recalculating proton dose directly on a CBCT. We did not fully optimize the CBCT imaging and its calibration to its full potential; therefore, the dose calculations were indicative but clearly suboptimal. Dose calculations directly on the CBCT require more-sophisticated methods to account for variability in patient size and imaging artifacts rather than a single calibration curve extracted from simplistic phantoms. This was, however, out of the scope of this study.

The results found for the dose similarity between dCT and rCT are promising for proton-therapy applications, even though significantly inferior to the IMRT cases. The estimation of the $IMPT_{3B}$ dose was less accurate in the region of the high-dose gradient but still showed good accuracy in the regions of highest clinical importance, (ie, the TV and OARs). We acknowledge that the lack of a perfect gold standard is the major limitation of our study. However, because there would still be setup errors between the CBCT and rCT scan, even if they were acquired on the same day (because the scanners are in different rooms), we did not think that extra and unnecessary (from a clinical perspective) imaging dose to the patient needed to acquire an extra CBCT on the same day as the rCT was justifiable. We believe that the effect of using an imperfect gold standard is more likely to have a negative than a positive impact on our results; that is, any mismatching between the rCT and the simulated CBCT should not help our method appear better than it really is. It is true that this could happen by chance, if the errors in registering the pCT to the simulated CBCT were the exact opposite of the errors when generating the simulated CBCT, but in our opinion this is unlikely. Furthermore, we have estimated the effect of using an imperfect gold standard by also performing the same dose analysis on a deformed CT resulting from warping the pCT to match the rCT (dCT_{rCT}). In such a case, the geometric information is correct; thus, the additional uncertainty caused by the incorrect gold standard should lay between the values reported in this article and the results found on the dCT_{rCT}. For proton plans, this additional uncertainty within the CBCT FoV was estimated to be approximately 5% and 1.5% of the pD for $DD_{2\%\text{-}pp}$ and DD_{RMS}, respectively. An additional limitation is the small patient sample used. Although the sample was appropriate for a proof-of-concept study such as this, follow-up studies with larger samples would be required to fully characterize the uncertainty of CBCT and DIR based "dose of the day" calculations.

The method proposed is of potential interest for adaptive proton therapy, but further work is necessary to address its poorer reliability in regions where the dose varies rapidly. We identified 3 major points that are crucial for CBCT- and DIR-based adaptive proton-therapy workflow and that can be further improved: (1) the registration algorithm, (2) the CBCT acquisition for adaptive radiation-therapy applications, and (3) the robustness of the treatment plan:

(1) Proton plans are more sensitive to inaccuracies in the registrations. Even though we used the state-of-art registration algorithm available in NiftyReg, that is a general-purpose algorithm designed to be applicable to a wide range of medical images from different modalities and on different parts of the anatomy. General-purpose algorithms can be made more realistic by incorporating additional constraints (eg, to avoid bone deformation [31]). Alternatively, algorithms specifically designed for the treatment site could be used, such as biomechanical-based algorithms that model the physical properties of the tissues being registered [32, 33]. Further work is also necessary to ensure the registration of (and attenuation by) the immobilization devices. For simplicity reasons, we removed the immobilization mask and treatment couch from the dose calculations, but the mask can contribute significantly to the attenuation of proton beams.
(2) The information acquired by the CBCT has to be adequate as missing important geometrical information due to limited FoV is concerning, particularly for adaptive proton therapy. Because the length of the CBCT scan is limited by the geometry of the system, acquiring 2 consecutive images may be the most appropriate solution for larger treatment volumes. Further improvement in the image quality will also facilitate the registrations.
(3) The $SFUD_{3B}$ and $IMPT_{5B}$ dose distributions were less sensitive to registration errors than the $IMPT_{3B}$ was, which can be related to the robustness of the plan. Robust treatment-plan optimization can result in plans that maintain target coverage and spare normal tissue in the presence of setup errors and range uncertainties [34]. Robust planning will have an important role in minimizing and accounting for the issues generated by the anatomic changes and could be used to make plans that are less sensitive to registration errors.

The level of accuracy necessary for the dose calculations will depend on the final application. For example, if the aim is to use the "dose of the day" to identify which patients may benefit from replanning, the accuracy requirements are not necessarily high because the decision to replan is being made clinically on a patient-by-patient basis. It is crucial for clinical translation to fully characterize the errors and uncertainties inherent in the dose calculations and to develop planning methods that account for them robustly.

This study assumes that CBCT imaging quality is the same as if the system was mounted on a linear-accelerator head, which may not be the case. The larger source-to-detector distance and the flex of the support system induced by gravity

increase the magnitude of the geometric deformation in comparison with photon systems and degrade the reconstruction process of the CBCT image [35]. The effect of such degradation will have to be verified once patient CBCT data during proton therapy becomes available. The lower image quality will most likely have more of an effect on dose calculations directly on the CBCT than it would on a dCT.

Even though the method proposed is still not optimal and can certainly be improved, it is clear that treatment adaptation in proton therapy is important, as shown by the dose differences between pCT and rCT. The range of proton beams within the patient needs to be predicted as accurately as possible not only during treatment planning but also throughout the treatment course. Knowledge of where the proton dose is being delivered throughout the treatment and online treatment adaptation is made possible by the introduction of CBCT imaging and has the potential to bring additional confidence to reduce the larger safety margins characteristic of proton therapy and, therefore, to fully use the potential advantages of this treatment modality [36]. The framework presented here is not exclusive to the head and neck and could be further extended to other anatomic sites of interest. However, site-specific validation work will be necessary because it is crucial for the DIR algorithm to be tailored for the specifics of the region being registered and the quality of the images acquired in such volumes.

Conclusions

We have presented a feasibility study investigating the use of CBCT and DIR for adaptive proton therapy. Even though the proposed method performed worse for proton therapy than it did for IMRT cases, accounting for anatomic changes is of additional importance in proton therapy, and the results found were promising. Improvements to registration, image acquisition, and planning strategies will allow for adaptive proton therapy based on daily CBCT.

ADDITIONAL INFORMATION AND DECLARATIONS

Conflicts of interest: The authors have no conflicts of interest to disclose.

Acknowledgments: Catarina Veiga was funded by Fundação para a Ciência e a Tecnologia grant (SFRH/BD/76169/2011), cofinanced by European Social Fund, Programa Operacional Potencial Humano, Quadro de Referência Estratégico Nacional and European Union. Jailan Alshaikhi was funded by the Royal Embassy of Saudi Arabia Cultural Bureau in the United Kingdom and Ireland and the Ministry of Higher Education of Saudi Arabia. Marc Modat and Sebastien Ourselin were supported by the National Institute of Health Research (NIHR) Comprehensive Biomedical Research Centre at University College London Hospitals and University College London grant 168. Jamie R. McClelland was supported by the Engineering and Physical Sciences Research Council's Intelligent Imaging Program Grant (EP/H046410/1).

References

1. Barker JL Jr, Garden AS, Ang KK, O'Daniel JC, Wang H, Court LE, Morrison WH, Rosenthal DI, Chao KS, Tucker SL, Mohan R, Dong L. Quantification of volumetric and geometric changes occurring during fractionated radiotherapy for head-and-neck cancer using an integrated CT/linear accelerator system. *Int J Radiat Oncol Biol Phys*. 2004;59:960–70.
2. Hansen EK, Bucci MK, Quivey JM, Weinberg V, Xia P. Repeat CT imaging and replanning during the course of IMRT for head-and-neck cancer. *Int J Radiat Oncol Biol Phys*. 2006;64:355–62.
3. Schwartz DL, Garden AS, Shah SJ, Chronowski G, Sejpal S, Rosenthal DI, Chen Y, Zhang Y, Zhang L, Wong PF, Garcia JA, Kian Ang K, Dong L. Adaptive radiotherapy for head and neck cancer—dosimetric results from a prospective clinical trial. *Radiother Oncol*. 2013;106:80–4.
4. Fotina I, Hopfgartner J, Stock M, Steininger T, Lutgendorf-Caucig C, Georg D. Feasibility of CBCT-based dose calculation: comparative analysis of HU adjustment techniques. *Radiother Oncol*. 2012;104:249–56.
5. Seabra J, Brousmiche S, Labarbe R, Vila M, Rit S, Wikler D, Lee J, Teo K, Orban de Xivry J, Macq B. *Design of Cone-Beam CT for Proton Therapy Gantry*. Louvain-La-Neuve, Belgium: Belgian Hospital Physicists Association Symposium; 2014.
6. Winey B, Park Y, Zhu M, Lu H-M, Moteabbed M, Sharp G. *Proton Gantry Mounted CBCT Development at Massachusetts General Hospital*. London, UK: National Physical Laboratory Proton Physics Research and Implementation Group Proton Therapy Physics Workshop; 2014.
7. Takao S, Shimizu S, Miyamoto N, Matsuura T, Toramatsu C, Nihongi H, Yamada T, Matsuda K, Sasaki T, Nagamine Y, Raba R, Umekawa T, Umegaki K, Shirato H. Commissioning of the on-board cone-beam CT system equipped on the

rotating gantry of a proton therapy system. Paper presented at: The 56th Annual Meeting of the American Association of Physicists in Medicine; July 20–24, 2014; Austin, TX.

8. Bolsi A, Lomax AJ, Pedroni E, Goitein G, Hug E. Experiences at the Paul Scherrer Institute with a remote patient positioning procedure for high-throughput proton radiation therapy. *Int J Radiat Oncol Biol Phys*. 2008;71:1581–90.
9. Lomax AJ, Goitein M, Adams J. Intensity modulation in radiotherapy: photons versus protons in the paranasal sinus. *Radiother Oncol*. 2003;66:11–8.
10. Steneker M, Lomax A, Schneider U. Intensity modulated photon and proton therapy for the treatment of head and neck tumors. *Radiother Oncol*. 2006;80:263–7.
11. Kandula S, Zhu X, Garden AS, Gillin M, Rosenthal DI, Ang KK, Mohan R, Amin MV, Garcia JA, Wu R, Sahoo N, Frank SJ. Spot-scanning beam proton therapy vs intensity-modulated radiation therapy for ipsilateral head and neck malignancies: a treatment planning comparison. *Med Dosim*. 2013;38:390–4.
12. Quan EM, Liu W, Wu R, Li Y, Frank SJ, Zhang X, Zhu XR, Mohan R. Preliminary evaluation of multifield and single-field optimization for the treatment planning of spot-scanning proton therapy of head and neck cancer. *Med Phys*. 2013;40: 081709.
13. Chan AW, Liebsch LJ, Deschler DG, Adams JA, Vrishali LV, McIntyre JF, Pommier P, Fabian RL, Busse PM. Proton radiotherapy for T4 nasopharyngeal carcinoma [abstract]. *J Clin Oncol*. 2004;22:5574.
14. Slater JD, Yonemoto LT, Mantik DW, Bush DA, Preston W, Grove RI, Miller DW, Slater JM. Proton radiation for treatment of cancer of the oropharynx: early experience at Loma Linda University Medical Center using a concomitant boost technique. *Int J Radiat Oncol Biol Phys*. 2005;62:494–500.
15. Nishimura H, Ogino T, Kawashima M, Nihei K, Arahira S, Onozawa M, Katsuta S, Nishio T. Proton-beam therapy for olfactory neuroblastoma. *Int J Radiat Oncol Biol Phys*. 2007;68:758–62.
16. Resto VA, Chan AW, Deschler DG, Lin DT. Extent of surgery in the management of locally advanced sinonasal malignancies. *Head Neck*. 2008;30:222–9.
17. Frank SJ, Cox JD, Gillin M, Mohan R, Garden AS, Rosenthal DI, Gunn GB, Weber RS, Kies MS, Lewin JS, Munsell MF, Palmer MB, Sahoo N, Zhang X, Liu W, Zhu XR. Multifield optimization intensity modulated proton therapy for head and neck tumors: a translation to practice. *Int J Radiat Oncol Biol Phys*. 2014;89:846–53.
18. Ramaekers BL, Pijls-Johannesma M, Joore MA, van den Ende P, Langendijk JA, Lambin P, Kessels AG, Grutters JP. Systematic review and meta-analysis of radiotherapy in various head and neck cancers: comparing photons, carbon-ions and protons. *Cancer Treat Rev*. 2011;37:185–201.
19. Simone CB, II, Ly D, Dan TD, Ondos J, Ning H, Belard A, O'Connell J, Miller RW, Simone NL. Comparison of intensity-modulated radiotherapy, adaptive radiotherapy, proton radiotherapy, and adaptive proton radiotherapy for treatment of locally advanced head and neck cancer. *Radiother Oncol*. 2011;101:376–82.
20. Veiga C, McClelland J, Moinuddin S, Lourenco A, Ricketts K, Annkah J, Modat M, Ourselin S, D'Souza D, Royle G. Toward adaptive radiotherapy for head and neck patients: Feasibility study on using CT-to-CBCT deformable registration for "dose of the day" calculations. *Med Phys*. 2014;41:031703.
21. Lomax NJ, Scheib SG. Quantifying the degree of conformity in radiosurgery treatment planning. *Int J Radiat Oncol Biol Phys*. 2003;55:1409–19.
22. Wang X, Zhang X, Dong L, Liu H, Gillin M, Ahamad A, Ang K, Mohan R. Effectiveness of noncoplanar IMRT planning using a parallelized multiresolution beam angle optimization method for paranasal sinus carcinoma. *Int J Radiat Oncol Biol Phys*. 2005;63:594–601.
23. D'Arienzo M, Masciullo SG, de Sanctis V, Osti MF, Chiacchiararelli L, Enrici RM. Integral dose and radiation-induced secondary malignancies: comparison between stereotactic body radiation therapy and three-dimensional conformal radiotherapy. *Int J Environ Res Public Health*. 2012;9:4223–40.
24. Rueckert D, Sonoda LI, Hayes C, Hill DL, Leach MO, Hawkes DJ. Nonrigid registration using free-form deformations: application to breast MR images. *IEEE Trans Med Imaging*. 1999;18:712–21.
25. Modat M, Daga P, Cardoso M, Ourselin S, Ridgway G, Ashburner J. Parametric non-rigid registration using a stationary velocity field [abstract]. In: *IEEE Workshop on Mathematical Methods in Biomedical Image Analysis*. Red Hook, NY: Curran Associates; 2012:145–50.
26. Veiga C, McClelland J, Moinuddin S, Ricketts K, Modat M, Ourselin S, D'Souza D, Royle G. Towards adaptive radiotherapy for head and neck patients: validation of an in-house deformable registration algorithm. *J Phys Conf Ser*. 2014;489:012083.

27. Yang Y, Schreibmann E, Li T, Wang C, Xing L. Evaluation of on-board kV cone beam CT (CBCT)-based dose calculation. *Phys Med Biol*. 2007;52:685–705.
28. Landry G, Dedes G, Zollner C, Handrack J, Janssens G, Orban de Xivry J, Reiner M, Paganelli C, Riboldi M, Kamp F, Sohn M, Wilkens JJ, Baroni G, Belka C, Parodi K. Phantom based evaluation of CT to CBCT image registration for proton therapy dose recalculation. *Phys Med Biol*. 2015;60:595–613.
29. Landry G, Nijhuis R, Dedes G, Handrack J, Thieke C, Janssens G, Orban de Xivry J, Reiner M, Kamp F, Wilkens JJ, Paganelli C, Riboldi M, Baroni G, Ganswindt U, Belka C, Parodi K. Investigating CT to CBCT image registration for head and neck proton therapy as a tool for daily dose recalculation. *Med Phys*. 2015;42:1354–66.
30. Lu W, Olivera GH, Chen Q, Ruchala KJ, Haimerl J, Meeks SL, Langen KM, Kupelian PA. Deformable registration of the planning image (kVCT) and the daily images (MVCT) for adaptive radiation therapy. *Phys Med Biol*. 2006;51:4357–74.
31. Kim J, Matuszak MM, Saitou K, Balter JM. Distance-preserving rigidity penalty on deformable image registration of multiple skeletal components in the neck. *Med Phys*. 2013;40:121907.
32. Bharatha A, Hirose M, Hata N, Warfield SK, Ferrant M, Zou KH, Suarez-Santana E, Ruiz-Alzola J, D'Amico A, Cormack RA, Kikinis R, Jolesz FA, Tempany CM. Evaluation of three-dimensional finite element-based deformable registration of pre- and intraoperative prostate imaging. *Med Phys*. 2001;28:2551–60.
33. Al-Mayah A, Moseley J, Hunter S, Velec M, Chau L, Breen S, Brock K. Biomechanical-based image registration for head and neck radiation treatment. *Phys Med Biol*. 2010;55:6491–500.
34. Stuschke M, Kaiser A, Abu Jawad J, Pottgen C, Levegrün S, Farr J. Multi-scenario based robust intensity-modulated proton therapy (IMPT) plans can account for set-up errors more effectively in terms of normal tissue sparing than planning target volume (PTV) based intensity-modulated photon plans in the head and neck region. *Radiat Oncol*. 2013;8:145.
35. Rosa Seabra JC, Brousmich S, Labarbe R, Lee JA, Macq B. Methodological study of geometric deformation for CBCT in proton therapy gantry. Paper presented at: Annual Symposium of the Institute of Electrical and Electronics Engineers, Engineering in Medicine and Biology Society; February 12, 2011; Brussels, Belgium.
36. Paganetti H. Range uncertainties in proton therapy and the role of Monte Carlo simulations. *Phys Med Biol*. 2012;57:R99–117.